



**HAL**  
open science

## From dome to duplex: Convergent gravitational collapse explains coeval intracratonic doming and nappe tectonics, central Australia

Youseph Ibrahim, Patrice Rey, Donna Whitney, Christian Teyssier, Françoise Roger, Valérie Bosse, Bénédicte Cenki

### ► To cite this version:

Youseph Ibrahim, Patrice Rey, Donna Whitney, Christian Teyssier, Françoise Roger, et al.. From dome to duplex: Convergent gravitational collapse explains coeval intracratonic doming and nappe tectonics, central Australia. *Geology*, 2024, 53 (3), pp.210-215. 10.1130/g51721.1 . hal-04401661

**HAL Id: hal-04401661**

**<https://hal.science/hal-04401661v1>**

Submitted on 18 Jan 2024

**HAL** is a multi-disciplinary open access archive for the deposit and dissemination of scientific research documents, whether they are published or not. The documents may come from teaching and research institutions in France or abroad, or from public or private research centers.

L'archive ouverte pluridisciplinaire **HAL**, est destinée au dépôt et à la diffusion de documents scientifiques de niveau recherche, publiés ou non, émanant des établissements d'enseignement et de recherche français ou étrangers, des laboratoires publics ou privés.

1 From dome to duplex: convergent gravitational collapse  
2 explains coeval intracratonic doming and nappe tectonics,  
3 central Australia

4 **Youseph Ibrahim<sup>1</sup>, Patrice F. Rey<sup>1</sup>, Donna L. Whitney<sup>2</sup>, Christian Teyssier<sup>2</sup>, Françoise**  
5 **Roger<sup>3</sup>, Valérie Bosse<sup>4</sup> and Bénédicte Cenki<sup>3</sup>**

6 <sup>1</sup>School of Geosciences, University of Sydney, NSW 2006, Australia

7 <sup>2</sup>Department of Earth Sciences, University of Minnesota, Minnesota 55455, USA

8 <sup>3</sup>Géosciences Montpellier, Université de Montpellier, CNRS, 34095 Montpellier cedex, France

9 <sup>4</sup>Laboratoire Magmas et Volcans, Campus Universitaire des Cézeaux, 63178 Aubière Cedex,  
10 France

11 **ABSTRACT**

12 In central Australia, an apparently coeval gneiss dome (Entia Dome) developed adjacent  
13 to a thrust belt (Arltunga Nappe Complex) within an intracratonic setting. Here we employ a  
14 combination of fieldwork, geochronology, and numerical modeling to investigate the structure  
15 and tectonic evolution of these features. We present a structural model linking an extensional  
16 domain comprising the Entia Dome, across a transitional zone containing the Bruna décollement  
17 zone and the Illogwa shear zone, into a contractional zone comprising thrusts and duplexes of the  
18 Arltunga Nappe Complex. Supported by numerical modeling, we propose a tectonic model in  
19 which the dome and nappe complex formed synchronously because of the convergent  
20 gravitational collapse of the 30-40 km deep Paleozoic Harts Range rift.

21 **INTRODUCTION**

22 Defying traditional plate tectonics, the Alice Springs Orogeny (ASO) developed between  
23 450 to 300 Ma deep within the interior of the Australian continent (Fig. 1), at significant  
24 distances from any plate boundaries. It spans ~600 km, following a WNW-ESE striking corridor  
25 amidst the weaker regions between the North, South, and West Australian cratons (Nixon et al.,  
26 2022). Before the ASO, a large portion of the Australian Paleoproterozoic interior remained  
27 buried beneath the Neoproterozoic to Devonian Centralian Superbasin, remnants of which

28 include the Amadeus Basin (Fig. 1). During much of the Palaeozoic Era, Australia existed as a  
29 Gondwana promontory bordered by active margins to the NW (Metcalf, 2021), N (Jost et al.,  
30 2018) and Pacific margins (Rosenbaum, 2018). Consequently, the intracratonic ASO has been  
31 attributed to a combination of mantle dynamics (Houseman and Molnar, 2001; Roberts and  
32 Houseman, 2001) and far-field stresses (Klootwijk, 2013; Silva et al., 2018).

33 The region NE of the Amadeus basin presents an intriguing geological association of the  
34 Entia gneiss dome, in which Paleoproterozoic upper amphibolite facies gneisses were exhumed  
35 alongside a series of nappes (Fig. 1). The nappe complex comprises the amphibolite to granulite  
36 facies rocks (10 kbar, 850°C; Hand et al., 1999; Mawby et al., 1999) of the Harts Range  
37 Metamorphic Complex (HRMC), the Paradise Nappes, and their lower-grade Neoproterozoic  
38 covers (Forman, 1971). These isoclinal fold nappes were thrust onto the greenschist facies Ruby  
39 Gap duplex and White Range duplex, which consist of Amadeus basin sequences, overlapping  
40 the Amadeus basin (Dunlap and Teyssier, 1995). Collectively, these nappes constitute the  
41 Arltunga Nappe Complex.

42 Understanding of the regional geology took a transformative turn when detrital zircon  
43 data revealed that the HRMC, into which the Entia dome was emplaced, did not belong to the  
44 Paleoproterozoic basement. Instead, these gneisses are the metamorphic equivalent of  
45 Neoproterozoic to Palaeozoic marine siliciclastic and limestone sediments of the Amadeus Basin  
46 with interlayered metavolcanics (Maidment et al., 2013; Tucker et al., 2015). Amphibolite to  
47 granulite facies metamorphism between 470 to 450 Ma is associated with bedding-parallel  
48 fabrics, suggesting syn-rift high-T metamorphism within the Harts Range Rift, a 30 to 40 km  
49 deep sub-basin adjacent to the Amadeus Basin (Hand et al., 1999; Mawby et al., 1999; Maidment  
50 et al., 2005; Tucker et al., 2015). Granulite facies conditions seem to have been confined to  
51 deeper parts of the Harts Range Rift, with little effect on the adjacent Paleoproterozoic basement  
52 (Mawby et al., 1999).

53 Episodic pegmatite emplacement between 450 and 300 Ma within the Entia Dome and  
54 the HRMC suggests the maintenance of high-T conditions in the deeper crust during most of the  
55 Paleozoic (Buick et al., 2008). Hence, the Entia Dome is a post-460 Ma structure that ascended  
56 through the HRMC during the ASO. The driver for protracted partial melting following an  
57 episode of high-grade metamorphism in this intracontinental setting remains enigmatic (Buick et  
58 al., 2008; Asimus et al., 2023).

59 This paper focuses on the structure and tectonic history of the region between the Entia  
60 Dome and the Ruby Gap Duplex (RGD) across the intervening Illogwa Shear Zone (ISZ; Fig. 1).  
61 We document a structural continuity from the Entia Dome to the RGD and argue that the dome  
62 and duplex, active between 340 and 310 Ma, represent an extensional and contractional domain,  
63 respectively, linked by a translational domain that consists of the Bruna Décollement Zone  
64 (BDZ) and the ISZ. We propose that the deep Harts Range rift basin led to a significant  
65 gravitational potential anomaly that relaxed via inward convergent gravitational collapse.

## 66 **A TRANSECT FROM DOME TO DUPLEX**

### 67 **Entia Dome**

68 The Entia Dome comprises migmatitic quartzofeldspathic gneisses and layered  
69 amphibolites and calc-silicates. A composite layer-parallel compositional banding fabric defines  
70 an internal architecture involving two subdomes separated by a planar high-strain zone (Fig. 1,  
71 2A). The subdome cores host the Huckitta and Inkamulla granodiorites dated (U-Pb zircon) at  
72 1762 Ma and 1773 Ma, respectively (Maidment et al., 2005). Both granodiorites display a  
73 magmatic to solid-state fabric concordant with overlying migmatitic gneisses. On average,  
74 lineations within the dome trend to the NE (Fig. 1) and plunge 20-30° to the NE. Polyphase  
75 structures in the migmatites show evidence of at least three fabric-forming events (Fig 2D-E),  
76 with a clear regional partitioning. In the dome, the metatexite compositional layering and layer  
77 parallel foliation is folded into tight to isoclinal recumbent folds, ranging from centimeter to 10's  
78 of meters in amplitude (Fig. S1A-B). The sub-horizontal migmatitic layering displays locally  
79 sub-horizontal asymmetric boudinage and low-angle extensional shear bands with melt  
80 segregation that points to a strong extensional tectonic regime above the solidus (Fig. S1C). The  
81 magmatic fabric in the granodiorites preserves remnants of older structures (Fig. S2). At the  
82 margin of the dome, the recumbent folds are refolded by cascading recumbent folds (Fig. S3).  
83 Granite-bearing extensional fractures, some axial planar to these second-generation folds, show  
84 that these folds also developed at temperatures above the solidus (Fig. 2D-E). In between the  
85 subdomes, the high-strain zone records a strong horizontal NW-SE shortening, with tight to  
86 isoclinal upright folds (Fig. S4). The strain distribution is consistent with that expected during  
87 the exhumation of a migmatitic-cored dome, with vertical shortening and horizontal extension on

88 top of the dome, gravity folding along its margin (Cruden, 1990), and horizontal shortening  
89 between the subdomes (Rey et al., 2017).

90 U-Pb ages of metamorphic monazite from Entia gneisses between 365 and 308 Ma  
91 (Wade et al., 2008 and references therein; Varga et al., 2021), as well as U-Pb ages of  
92 metamorphic zircon growth in the Huckitta Granodiorite at  $\sim 332 \pm 3$  Ma (Maidment et al., 2005)  
93 and  $\sim 330 \pm 6$  Ma (Hand et al., 1999) point to a protracted metamorphism from 360 to 310 Ma,  
94 peaking at 7-9 kbar and 680-720°C (Varga et al., 2021 and references therein) and melt present  
95 conditions (Asimus et al., 2023). To better constrain the age of deformation, we conducted U-Th-  
96 Pb LA-ICPMS geochronology (Fig. S8) on monazite from a folded leucocratic vein within a  
97 metatexite between the subdomes (Figs. 1, 2D, S4). Two distinct date populations identified at  
98  $339 \pm 4$  Ma and  $314 \pm 4$  Ma, as well as a concordant date at  $365 \pm 8$  Ma, are interpreted as two  
99 pulses of doming and melt extraction during a  $\sim 365$  Ma to 310 Ma period of protracted  
100 metamorphism, melting and deformation.

#### 101 **South Margin of the Entia Dome**

102 The Bruna décollement zone deforms the contact between the Paleoproterozoic Entia  
103 gneisses and the Neoproterozoic to Paleozoic Irindina Gneiss at the base of the HRMC (Fig. 1)  
104 (James et al., 1989). Separating the basement and cover, the Bruna Granitic Gneiss (BGG) (Fig.  
105 S5) has been interpreted as a  $\sim 1745$  Ma (U/Pb zircon) laccolith (Ding and James, 1985;  
106 Mortimer et al., 1987; Cooper et al., 1988). The BGG records heterogeneous deformation (James  
107 et al., 1989). Along the S margin of the Entia Dome, the BDZ corresponds to a prominent S-  
108 dipping normal shear zone. A strong L-S fabric carries a mineral and stretching lineation  
109 plunging to the SSW (Fig. 2F). Sm/Nd whole rock-garnet-hornblende isochron dating of BGG  
110 from the sheared NW margin of the Entia Dome yielded an age of  $449 \pm 10$  Ma, interpreted to  
111 reflect a phase of Ordovician deformation (Mawby et al., 1999). Similar ages have been reported  
112 in the Harts Range (e.g., Buick et al., 2008). To constrain the age of shearing along the S margin  
113 of the dome, we have performed *in situ* LA-ICPMS U-Pb dating of titanite from an isoclinally  
114 folded aplite vein (Fig. 2C) hosted in sheared BGG (Fig. 1). We obtained a date of  $315 \pm 4$  Ma  
115 (Fig. S8), interpreted as the minimum emplacement age for the vein and maximum age for  
116 shearing and folding, closely agreeing with the  $314 \pm 4$  Ma age obtained in the high-strain zone  
117 between the subdomes.

118 South of the Entia Dome, the BDZ flattens into a broad synform (Fig. 2A). The L-S  
119 fabric is flat-lying, with the prominent stretching lineation gently plunging to the SSW or NNE.  
120 In some localities, strain shadows around K-feldspar and S-C fabrics in the BGG support a top-  
121 to-the-SW sense of shear (Fig. S6A-B). However, deformation was heterogeneous, varying in  
122 intensity and involving both simple and pure shear (Fig. S6C). Underlying the BGG, the  
123 Strangways gneisses are exposed in the core of a few discrete antiforms (Fig. 1). The BGG thins  
124 out above the roof thrust of the duplex (Fig. 2).

### 125 **Ruby Gap duplex and the Illogwa shear zone**

126 South of the BGG, the ISZ consists of quartzofeldspathic gneisses and schists, with mafic  
127 and calc-silicate interlayering, reminiscent of the rocks in the Entia Dome. The foliation dips 30-  
128 50° to the N and carries a down-dip stretching and muscovite lineation. We have observed S-C  
129 fabrics,  $\delta$ -clasts, and  $\sigma$ -clasts recording clear top-to-the-SW kinematics (Fig. 2E, Fig. S7). This  
130 shear zone is in structural conformity with the overlying upper amphibolite facies BDZ to the N  
131 and the underlying greenschist facies RGD to the S. Although the ISZ is often presented as a  
132 retrograde shear zone (Foden et al., 1995), it is part of an inverted metamorphic gradient linking  
133 the upper-amphibolite facies at the Entia Dome's S margin to the greenschist facies fabric of the  
134 RGD (Collins and Teyssier, 1989; Dunlap and Teyssier, 1995). We speculate that the ISZ fabric  
135 is the axial planar fabric of an anticlinal fold nappe made mainly of Paleoproterozoic gneisses,  
136 which could be structurally underneath the Paradise Nappes (Figs. 2, 3).  $^{207}\text{Pb}/^{206}\text{Pb}$  zircon ages  
137 of  $1794 \pm 6$  Ma and  $1769 \pm 3$  Ma are interpreted as crystallization ages and later alteration,  
138 respectively. In contrast, the  $327 \pm 2$  Ma  $^{40}\text{Ar}-^{39}\text{Ar}$  age obtained on muscovite (Reno and Fraser,  
139 2021) defining the lineation (Fig. S7) can be interpreted as the age of the ASO fabric.

140 Underneath and in structural conformity with the ISZ, the RGD is a S-directed duplex  
141 comprising Amadeus basin sequences and the underlying Paleoproterozoic basement. To the  
142 West, it occupies the lowest structural level of the Arltunga Nappe Complex, underlying the  
143 Paradise and HRMC nappes and coeval with the structurally equivalent White Range duplex  
144 (Dunlap and Teyssier, 1995) (Fig. 1). To the first order, what is preserved is the duplicated limb  
145 of an anticlinal fold nappe (Fig. 2A). The basement and the competent Heavitree Quartzite are  
146 attached, and the overlying incompetent Bitter Springs Fm (Fig. 2B) acts as a décollement.  
147 Thrusting occurred between 336 and 311 Ma ( $^{40}\text{Ar}-^{39}\text{Ar}$  on white mica) at temperatures

148 straddling the ductile-brittle transition (250-300 °C; Dunlap, 1997). Under these conditions,  
149 thrust sheets internally deform by stretching in the transport direction.

## 150 **Summary**

151 The structure across our transect consists of the Entia Dome with a double-dome  
152 architecture, adjacent to the Arltunga Nappe Complex to the S, comprising a stack of imbricated  
153 metamorphic fold nappes including the ISZ (Figs. 2A, 3). The structural geology is conformal,  
154 with a progressive decrease in metamorphic conditions from upper amphibolite facies in the  
155 Entia Dome and the BGG, to lower amphibolite facies across the ISZ and greenschist facies in  
156 the RGD (Figs. 2A, 3). Structures within the Entia Dome and the BDZ developed under  
157 extension, while the Arltunga Nappe Complex developed under contraction. Exhumation of the  
158 Entia Dome, shearing along the BDZ and ISZ, and thrusting of the Arltunga Nappe Complex are  
159 age-bracketed between ~345 and ~310 Ma. The structural continuity and geochronology indicate  
160 that these features are synchronous and interrelated.

## 161 **TECTONIC MODEL**

162 The Entia Dome was emplaced into the 30-40 km deep Harts Range Rift basin (i.e.,  
163 Irindina Province), the base of which reached granulite facies metamorphism and melting at  
164 ~470 Ma (Maidment et al., 2013; Tucker et al., 2015). The density contrast between the  
165 Neoproterozoic to Paleozoic sedimentary basin infill and the metamorphic Paleoproterozoic  
166 basement creates a strong horizontal pressure gradient, leading to significant gravitational  
167 stresses acting laterally towards the basin (Rey et al., 2001). As the geotherm in the basin  
168 reached melting conditions, these gravitational forces may have overcome viscous strength to  
169 drive centripetal flow, forcing the exhumation of the Entia Dome and the development of gravity  
170 nappes.

171 To test this hypothesis, we ran a set of thermal-mechanical numerical experiments using  
172 the *Underworld* framework (Moresi et al. 2007). The model setup comprises a 34 km deep rift  
173 basin, embedded into a metamorphic basement overlying a viscous mantle (Fig. 4A). The  
174 temperature field reflects conditions at ~470 Ma and delivers partial melting in the deeper level  
175 of the basin as well as the basement. Rheology is temperature, stress, strain, strain rate and melt  
176 dependent. Detailed model information is provided in the data repository.

177 We have tested static, mild, and faster convergent and divergent velocity conditions. All  
178 sets of experiments lead to the exhumation of a basement-cored double-dome, pushing the basin  
179 infill upward and laterally into gravity nappes (Fig. 4B-D). This experiment (Fig. 4) suggests that  
180 the contractional collapse of the Harts Range Rift basin exhumed the Entia Dome and triggered  
181 S-SW gliding of gravity-driven fold nappes, accommodated by isoclinal folding and foliation-  
182 parallel slip. At cooler conditions, limbs of the isoclinal fold nappes are imbricated forming the  
183 RGD and White Range duplex. A transitional domain links the extensional exhumation of the  
184 dome to the contractional deformation at the front of the nappe complex (Fig. 4D). The delay  
185 between granulite facies conditions at 470-450 Ma and doming at ~340-310 Ma may be due to  
186 rifting's divergent velocity balancing the convergent gravitational velocity until ~355 Ma and  
187 slow conductive heating delaying basement weakening and convergent flow.

## 188 **CONCLUSIONS**

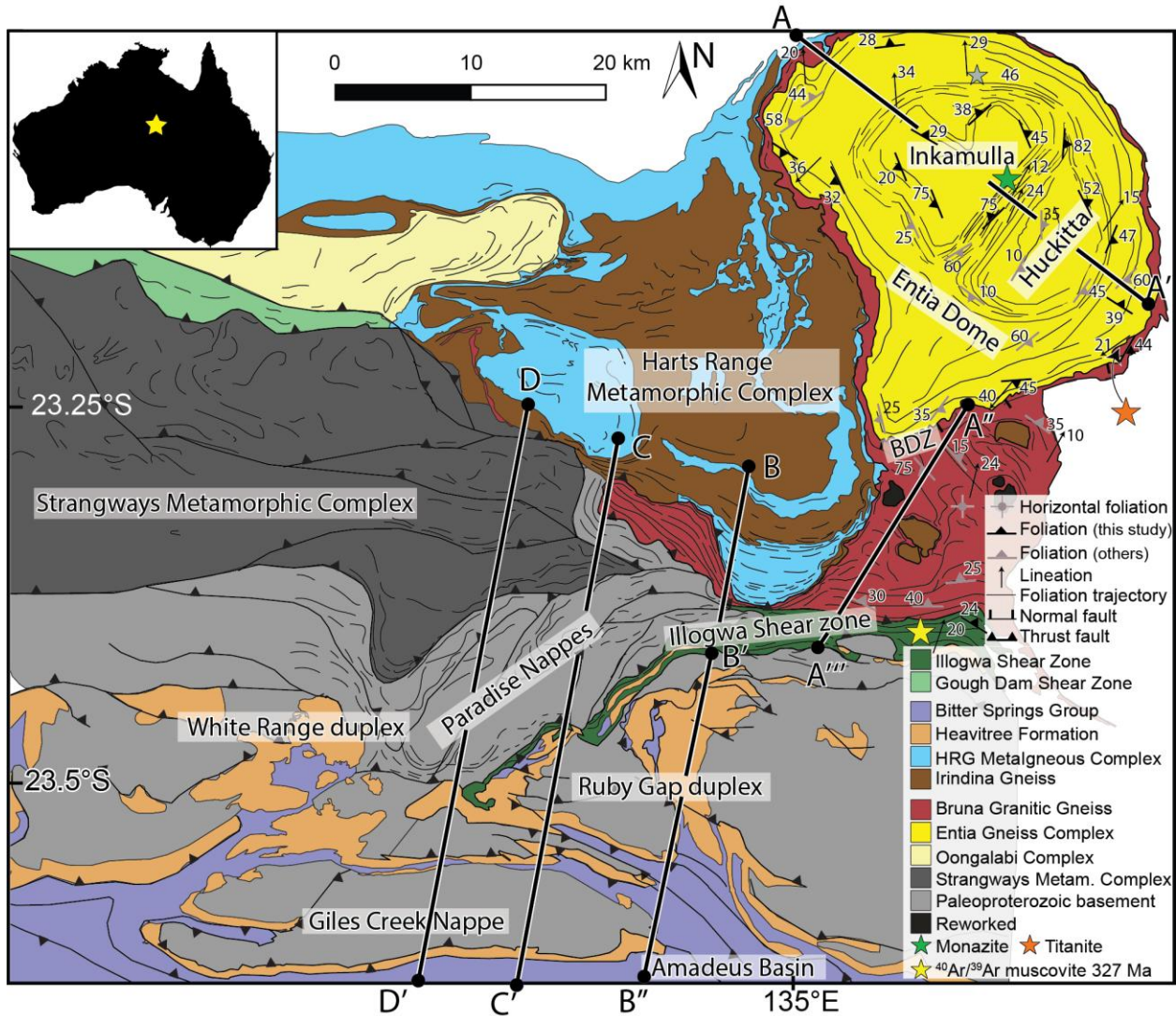
189 We propose a tectonic model linking the Entia Dome and the RGD based on i/ the  
190 structural and metamorphic continuity between the dome and the duplex, ii/ geochronological  
191 constraints showing synchronous dome exhumation and nappe emplacement from ~340 to ~310  
192 Ma, and iii/ coupled thermo-mechanical numerical experiments illustrating the geodynamics.  
193 Our model invokes the contractional gravitational collapse of the Neoproterozoic to Devonian  
194 Harts Range Rift basin as the driver for exhumation of the Entia dome, associated with  
195 gravitational spreading of the basin infill. This gravity-driven deformation was superimposed on  
196 far-field stresses driven by plate tectonics and may have contributed to deformation along the N  
197 margin of the Amadeus basin. While the processes described here explain some Carboniferous  
198 features observed in the east Arunta region, it cannot explain the totality of the ASO strain field.

## 199 **ACKNOWLEDGMENTS**

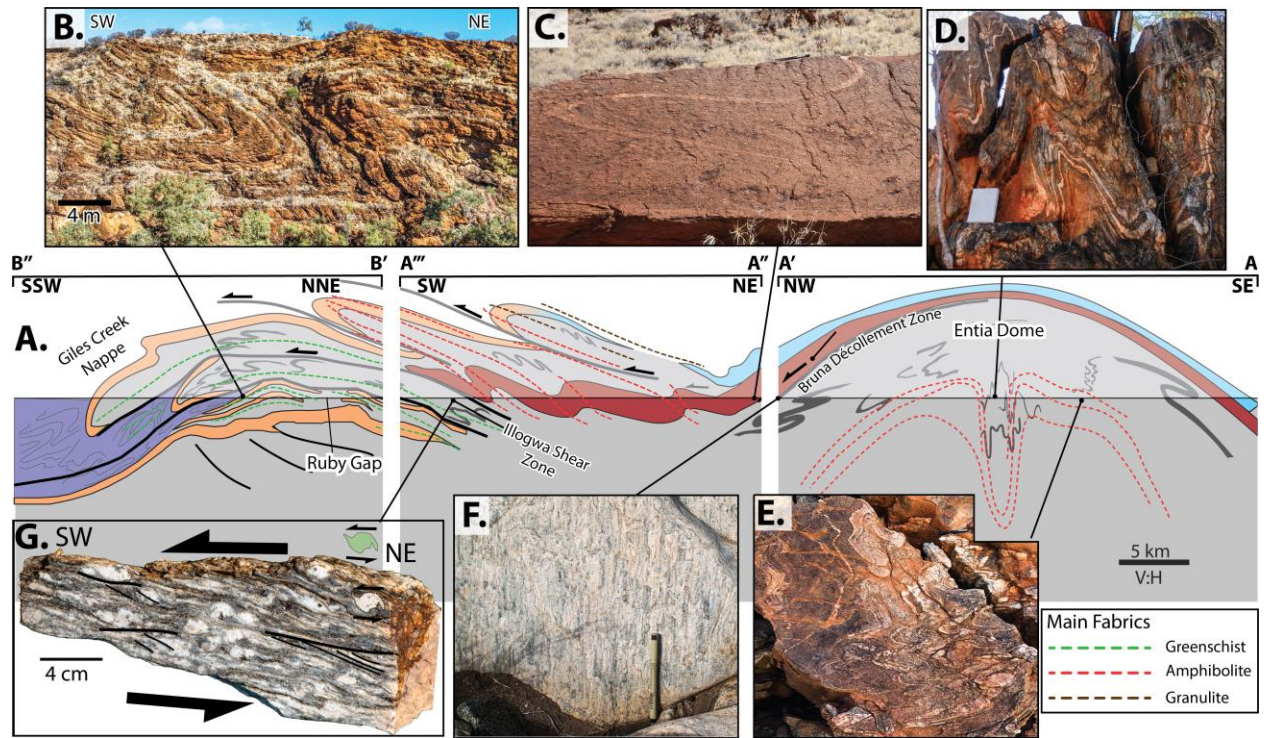
200 We acknowledge funding by Australian Research Council grants ARC-LP190100146 and ARC-  
201 DP220100709, and support by NCI's National Computational Merit Allocation Scheme, Pawsey  
202 Supercomputing Centre, and Underworld provided by AuScope. B.C. received funding from  
203 European Horizon 2020 grant no. 793978. We thank our reviewers for their comments and  
204 insights.

205

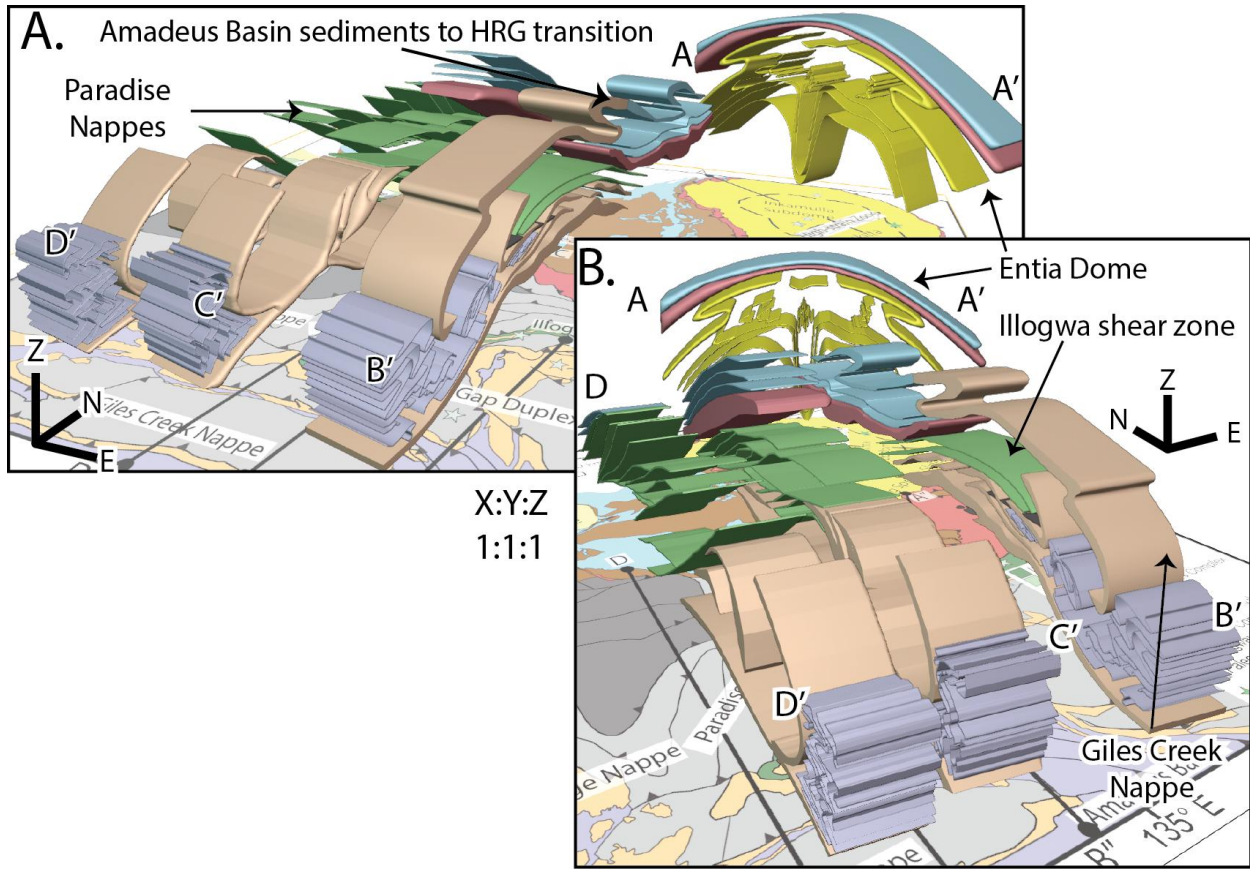




207  
 208 Figure 1. Geological map of the study area, central Australia, including location of  
 209 geochronology data ( $^{40}\text{Ar}/^{39}\text{Ar}$  on muscovite from Reno and Fraser, 2021), using a combination  
 210 of our own data and data from Forman (1971), Shaw et al. (1984), Shaw and Freeman (1990),  
 211 and Dunlap (1992). HRG—Harts Range Group.

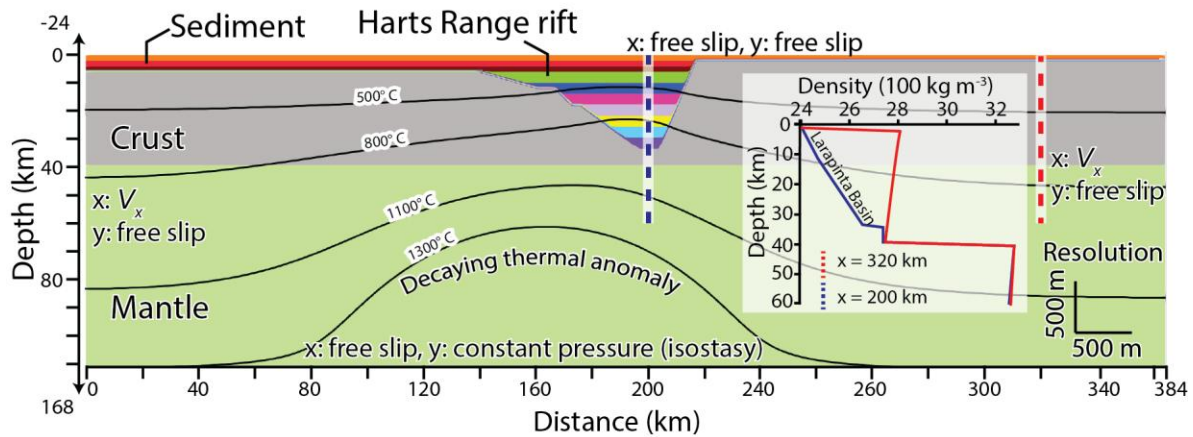


212  
 213 Figure 2. (A) Composite cross section from Ruby Gap Duplex to Entia Dome. Major thrust faults  
 214 are shown as thick black lines. Lighter shading indicates interpretation above the current  
 215 topography. The Harts Range Metamorphic Complex, including the Irindina Gneiss, is shown in  
 216 light blue. Section lines and legend are shown in Figure 1. (B) Folds in the Bitter Springs Group.  
 217 (C) Folded aplite vein with axial planar foliation in the Bruna décollement zone (pen for scale).  
 218 (D, E) Upright folds (notebook for scale) (D) refolded into cascading folds (pen for scale) (E) in  
 219 the high-strain dome envelope. (F) L-S tectonite within the Bruna décollement zone. (G)  
 220 Kinematic indicators in the Illogwa shear zone.

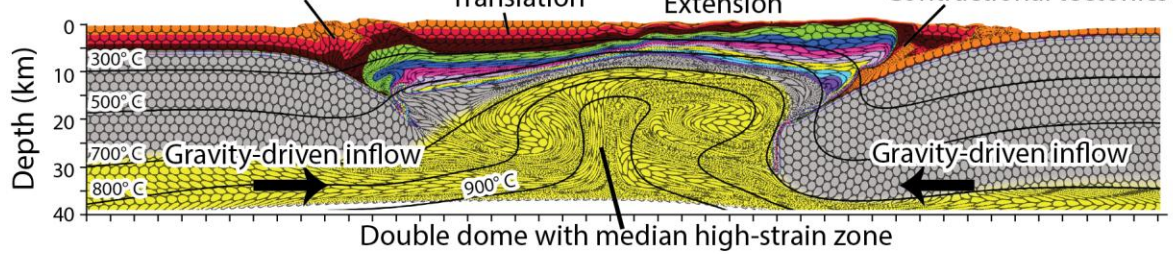


221  
 222 Figure 3. Two schematic views of the structural architecture of Entia Dome and Arltunga Nappe  
 223 Complex. Paradise Nappes are colored green. Legend and section lines are shown in Figure 1.  
 224 HRG—Harts Range Group.

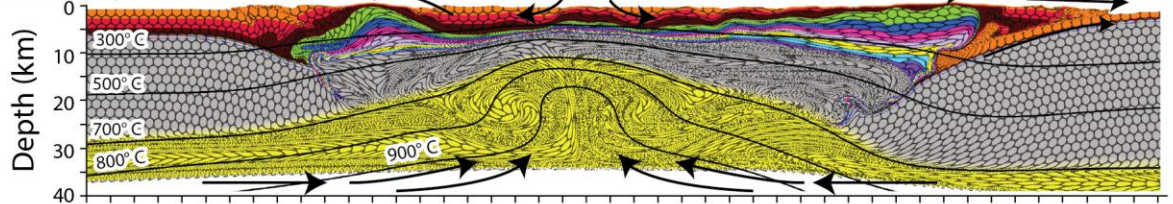
A. 0 m.y. Pre-doming lithosphere architecture



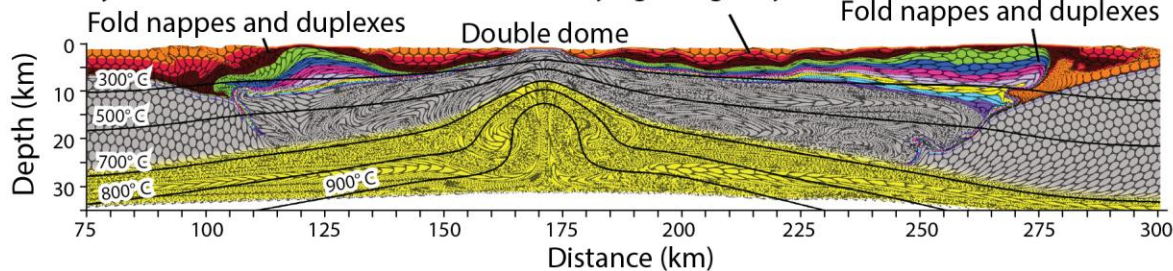
B. 3.4 m.y. Contractional tectonics



C. 6.7 m.y.



D. 10 m.y.



225  
 226 Figure 4. Numerical experiment showing contractional gravitational collapse of a deep and hot  
 227 rift basin triggering exhumation of a gneiss dome and associated gravity nappes. (A) Initial  
 228 model setup showing materials distribution, density profiles, boundary conditions, and isotherms.  
 229 Velocity boundary condition  $V_x$  is applied to both vertical walls.  $V_x$  is compressional at  $0.05$   
 230  $\text{mm yr}^{-1}$  for 4 m.y. and extensional at  $0.5 \text{ cm yr}^{-1}$  for the following 6 m.y. Decaying heat  
 231 anomaly approximates temperature conditions associated with rifting. Blue and red dashed lines

232 show locations of density profile. (B–D) Model evolution. Finite strain ellipses and isotherms are  
233 overlaid on the deforming material. Thin black arrows show flow direction.

## 234 REFERENCES

235 Asimus, J.L., Daczko, N.R., and Ezad, I.S., 2023, Melt-present deformation at the Entia Dome,  
236 Central Australia: A metamorphic core complex formed during lower crustal tectonic extrusion:  
237 *Lithos*, v. 448–449, <https://doi.org/10.1016/j.lithos.2023.107170>.

238 Buick, I.S., Storkey, A., and Williams, I.S., 2008, Timing relationships between pegmatite  
239 emplacement, metamorphism and deformation during the intra-plate Alice Springs Orogeny,  
240 central Australia: *Journal of Metamorphic Geology*, v. 26, p. 915–936,  
241 <https://doi.org/10.1111/j.1525-1314.2008.00794.x>.

242 Collins, W.J., and Teyssier, C., 1989, Crustal scale ductile fault systems in the Arunta Inlier,  
243 central Australia: *Tectonophysics*, v. 158, p. 49–66, [https://doi.org/10.1016/0040-](https://doi.org/10.1016/0040-1951(89)90314-4)  
244 [1951\(89\)90314-4](https://doi.org/10.1016/0040-1951(89)90314-4).

245 Cooper, J.A., Mortimer, G.E., and James, P.R., 1988, Rate of Arunta Inlier evolution at the  
246 eastern margin of the Entia Dome, central Australia: *Precambrian Research*, v. 40–41, p. 217–  
247 231, [https://doi.org/10.1016/0301-9268\(88\)90069-1](https://doi.org/10.1016/0301-9268(88)90069-1).

248 Cruden, A.R., 1990, Flow and fabric development during the diapiric rise of magma: *The Journal*  
249 *of Geology*, v. 98, p. 681–698, <https://doi.org/10.1086/629433>.

250 Ding, P., and James, P.R., 1985, Structural evolution of the Harts Range Area and its  
251 implication for the development of the Arunta Block, central Australia: *Precambrian Research*,  
252 v. 27, p. 251–276, [https://doi.org/10.1016/0301-9268\(85\)90015-4](https://doi.org/10.1016/0301-9268(85)90015-4).

253 Dunlap, W.J., 1992, Structure, kinematics, and cooling history of the Arltunga Nappe Complex,  
254 central Australia [Ph.D. thesis]: University of Minnesota, 276 p.

255 Dunlap, W.J., 1997, Neocrystallization or cooling?  $^{40}\text{Ar}/^{39}\text{Ar}$  ages of white micas from low-  
256 grade mylonites: *Chemical Geology*, v. 143, p. 181–203, [https://doi.org/10.1016/S0009-](https://doi.org/10.1016/S0009-2541(97)00113-7)  
257 [2541\(97\)00113-7](https://doi.org/10.1016/S0009-2541(97)00113-7).

258 Dunlap, W.J., and Teyssier, C., 1995, Thermal and structural evolution of the intracratonic  
259 Arltunga Nappe Complex, central Australia: *Tectonics*, v. 14, p. 1182–1204,  
260 <https://doi.org/10.1029/95TC00335>.

261 Foden, J., Mawby, J., Kelley, S., Turner, S., and Bruce, D., 1995, Metamorphic events in the  
262 eastern Arunta Inlier, Part 2. Nd-Sr-Ar isotopic constraints: *Precambrian Research*, v. 71, p. 207–  
263 227, [https://doi.org/10.1016/0301-9268\(94\)00062-V](https://doi.org/10.1016/0301-9268(94)00062-V).

264 Forman, D.J., 1971, The Arltunga Nappe Complex, Macdonnell Ranges, Northern Territory,  
265 Australia: *Journal of the Geological Society of Australia*, v. 18, p. 173–182,  
266 <https://doi.org/10.1080/00167617108728756>.

267 Hand, M., Mawby, J.O., Kinny, P., and Foden, J., 1999, U–Pb ages from the Harts Range,  
268 central Australia: Evidence for early Ordovician extension and constraints on Carboniferous  
269 metamorphism: *Journal of the Geological Society*, v. 156, p. 715–730,  
270 <https://doi.org/10.1144/gsjgs.156.4.0715>.  
271  
272 Houseman, G., and Molnar, P., 2001, Mechanisms of lithospheric rejuvenation associated with  
273 continental orogeny, in Miller, J.A., et al., eds., *Continental Reactivation and Reworking*:  
274 Geological Society, London, Special Publication 184, p. 13–38,  
275 <https://doi.org/10.1144/GSL.SP.2001.184.01.02>.  
276  
277 James, P.R., Macdonald, P., and Parker, M., 1989, Strain and displacement in the Harts Range  
278 detachment zone: A structural study of the Bruna Gneiss from the western margin of the Entia  
279 Dome, central Australia: *Tectonophysics*, v. 158, p. 23–48, [https://doi.org/10.1016/0040-](https://doi.org/10.1016/0040-1951(89)90313-2)  
280 [1951\(89\)90313-2](https://doi.org/10.1016/0040-1951(89)90313-2).  
281  
282 Jost, B.M., Webb, M., and White, L.T., 2018, The Mesozoic and Palaeozoic granitoids of north-  
283 western New Guinea: *Lithos*, v. 312–313, p. 223–243,  
284 <https://doi.org/10.1016/j.lithos.2018.04.027>.  
285  
286 Klootwijk, C., 2013, Middle–Late Paleozoic Australia-Asia convergence and tectonic extrusion  
287 of Australia: *Gondwana Research*, v. 24, p. 5–54, <https://doi.org/10.1016/j.gr.2012.10.007>.  
288  
289 Maidment, D.W., Hand, M., and Williams, I.S., 2005, Tectonic cycles in the Strangways  
290 Metamorphic Complex, Arunta Inlier, central Australia: Geochronological evidence for  
291 exhumation and basin formation between two high-grade metamorphic events: *Australian*  
292 *Journal of Earth Sciences*, v. 52, p. 205–215, <https://doi.org/10.1080/08120090500139414>.  
293  
294 Maidment, D.W., Hand, M., and Williams, I.S., 2013, High grade metamorphism of sedimentary  
295 rocks during Palaeozoic rift basin formation in central Australia: *Gondwana Research*, v. 24,  
296 p. 865– 885, <https://doi.org/10.1016/j.gr.2012.12.020>.  
297  
298 Mawby, J., Hand, M., and Foden, J., 1999, Sm-Nd evidence for high-grade Ordovician  
299 metamorphism in the Arunta Block, central Australia: *Journal of Metamorphic Geology*, v. 17,  
300 p. 653–668, <https://doi.org/10.1046/j.1525-1314.1999.00224.x>.  
301  
302 Metcalfe, I., 2021, Multiple Tethyan ocean basins and orogenic belts in Asia: *Gondwana*  
303 *Research*, v. 100, p. 87–130, <https://doi.org/10.1016/j.gr.2021.01.012>.  
304  
305 Moresi, L., Quenette, S., Lemiale, V., Mériaux, C., Appelbe, B., and Mühlhaus, H.-B., 2007,  
306 Computational approaches to studying non-linear dynamics of the crust and mantle: *Physics of*  
307 *the Earth and Planetary Interiors*, v. 163, p. 69–82, <https://doi.org/10.1016/j.pepi.2007.06.009>.  
308  
309 Mortimer, G.E., Cooper, J.A., and James, P.R., 1987, U-Pb and Rb-Sr geochronology and  
310 geological evolution of the Harts Range ruby mine area of the Arunta Inlier, central Australia:  
311 *Lithos*, v. 20, p. 445–467, [https://doi.org/10.1016/0024-4937\(87\)90029-6](https://doi.org/10.1016/0024-4937(87)90029-6).

312 Nixon, A.L., Glorie, S., Fernie, N., Hand, M., De Vries Van Leeuwen, A.T., Collins, A.S.,  
313 Hasterok, D., and Fraser, G., 2022, Intracontinental fault reactivation in high heat production  
314 areas of central Australia: Insights from apatite fission track thermochronology: *Geochemistry,*  
315 *Geophysics, Geosystems*, v. 23, <https://doi.org/10.1029/2022GC010559>.  
316

317 Reno, B.L., and Fraser, G.L., 2021, Summary of results—Joint NTGS-GA geochronology  
318 project: Constraining cooling and deformation in the eastern Aileron Province through  
319  $^{40}\text{Ar}/^{39}\text{Ar}$  stepheating of hornblende, muscovite, and biotite: *Northern Territory Geological*  
320 *Survey Record 2021-001*, <https://geoscience.nt.gov.au/gemis/ntgsjspui/handle/1/91246>.  
321

322 Rey, P., Vanderhaeghe, O., and Teyssier, C., 2001, Gravitational collapse of the continental  
323 crust: Definition, regimes and modes: *Tectonophysics*, v. 342, p. 435–449,  
324 [https://doi.org/10.1016/S0040-1951\(01\)00174-3](https://doi.org/10.1016/S0040-1951(01)00174-3).  
325

326 Rey, P.F., Mondy, L., Duclaux, G., Teyssier, C., Whitney, D.L., Bocher, M., and Prigent, C.,  
327 2017, The origin of contractional structures in extensional gneiss domes: *Geology*, v. 45, p. 263–  
328 266, <https://doi.org/10.1130/G38595.1>.  
329

330 Roberts, E.A., and Houseman, G.A., 2001, Geodynamics of central Australia during the  
331 intraplate Alice Springs Orogeny: Thin viscous sheet models, in Miller, J.A., et al., eds.,  
332 *Continental Reactivation and Reworking: Geological Society, London, Special Publication 184*,  
333 p. 139–164, <https://doi.org/10.1144/GSL.SP.2001.184.01.08>.  
334

335 Rosenbaum, G., 2018, The Tasmanides: Phanerozoic tectonic evolution of eastern Australia:  
336 *Annual Review of Earth and Planetary Sciences*, v. 46, p. 291–325,  
337 <https://doi.org/10.1146/annurev-earth-082517-010146>.  
338

339 Shaw, R.D., and Freeman, M.J., 1990, Quartz, Northern Territory, sheet 5951: Australia Bureau  
340 of Mineral Resources, Geology and Geophysics, scale 1:100,000, <https://geoscience.nt.gov.au/gemis/ntgsjspui/handle/1/81611>.  
341

342 Shaw, R.D., Stewart, A.J., and Rickard, M.J., 1984, Arltunga–Harts Range region, Northern  
343 Territory: Australia Bureau of Mineral Resources, Geology and Geophysics, scale 1:100,000,  
344 <https://geoscience.nt.gov.au/gemis/ntgsjspui/handle/1/81909>.  
345

346 Silva, D., Piazzolo, S., Daczko, N.R., Houseman, G., Raimondo, T., and Evans, L., 2018,  
347 Intracontinental orogeny enhanced by far-field extension and local weak crust: *Tectonics*, v. 37,  
348 p. 4421–4443, <https://doi.org/10.1029/2018TC005106>.  
349

350 Tucker, N.M., Hand, M., and Payne, J.L., 2015, A rift-related origin for regional medium-  
351 pressure, high-temperature metamorphism: *Earth and Planetary Science Letters*, v. 421, p. 75–  
352 88, <https://doi.org/10.1016/j.epsl.2015.04.003>.  
353

354 Varga, J., Raimondo, T., Morrissey, L., Kelsey, D.E., and Hand, M., 2021, Pressure–  
355 temperature–time constraints on gneiss dome formation in an intracontinental orogen: *Journal of*  
356 *Metamorphic Geology*, v. 40, p. 457–488, <https://doi.org/10.1111/jmg.12635>.  
357

358 Varga, J., Raimondo, T., Hand, M., Curtis, S., and Daczko, N., 2022, Hydration, melt production  
359 and rheological weakening within an intracontinental gneiss dome: *Lithos*, v. 432–433, [https://](https://doi.org/10.1016/j.lithos.2022.106872)  
360 [doi.org/10.1016/j.lithos.2022.106872](https://doi.org/10.1016/j.lithos.2022.106872).

361

362 Wade, B.P., Hand, M., Maidment, D.W., Close, D.F., and Scrimgeour, I.R., 2008, Origin of  
363 metasedimentary and igneous rocks from the Entia Dome, eastern Arunta region, central  
364 Australia: A U-Pb LA-ICPMS, SHRIMP and Sm-Nd isotope study: *Australian Journal of Earth*  
365 *Sciences*, v. 55, p. 703–719, <https://doi.org/10.1080/08120090801982868>.